Propagation of Action Potentials in Dendrites Depends on Dendritic Morphology

PHILIPP VETTER,[1,*] ARND ROTH,[2,*] AND MICHAEL HÄUSSER[1]

[1]*Department of Physiology, University College London, London WC1E 6BT, United Kingdom; and*
[2]*Abteilung Zellphysiologie, Max-Planck-Institut für Medizinische Forschung, D-69120 Heidelberg, Germany*

Vetter, Philipp, Arnd Roth, and Michael Häusser. Propagation of action potentials in dendrites depends on dendritic morphology. *J Neurophysiol* 85: 926–937, 2001. Action potential propagation links information processing in different regions of the dendritic tree. To examine the contribution of dendritic morphology to the efficacy of propagation, simulations were performed in detailed reconstructions of eight different neuronal types. With identical complements of voltage-gated channels, different dendritic morphologies exhibit distinct patterns of propagation. Remarkably, the range of backpropagation efficacies observed experimentally can be reproduced by the variations in dendritic morphology alone. Dendritic geometry also determines the extent to which modulation of channel densities can affect propagation. Thus in Purkinje cells and dopamine neurons, backpropagation is relatively insensitive to changes in channel densities, whereas in pyramidal cells, backpropagation can be modulated over a wide range. We also demonstrate that forward propagation of dendritically initiated action potentials is influenced by morphology in a similar manner. We show that these functional consequences of the differences in dendritic geometries can be explained quantitatively using simple anatomical measures of dendritic branching patterns, which are captured in a reduced model of dendritic geometry. These findings indicate that differences in dendritic geometry act in concert with differences in voltage-gated channel density and kinetics to generate the diversity in dendritic action potential propagation observed between neurons. They also suggest that changes in dendritic geometry during development and plasticity will critically affect propagation. By determining the spatial pattern of action potential signaling, dendritic morphology thus helps to define the size and interdependence of functional compartments in the neuron.

INTRODUCTION

The propagation of action potentials in the dendritic tree has been the subject of great interest for over a century, beginning with the speculations of Ramón y Cajal (1904) on the directional flow of signals in neurites. During the past few decades, evidence has accumulated to suggest that under most conditions, the sodium action potential (AP), the output signal of the neuron, is initiated in the axon and retrogradely invades the dendritic tree, a process known as backpropagation (reviewed by Stuart et al. 1997b). Backpropagation has been demonstrated in a variety of different cell types in vitro, and evidence for backpropagation in vivo has been provided by recordings in both anesthetized (Helmchen et al. 1999; Svoboda et al. 1997,

1999) and awake animals (Buzsaki and Kandel 1998). APs can also be initiated in the dendrites under conditions of intense synaptic stimulation (Chen et al. 1997; Golding and Spruston 1998; Kamondi et al. 1998; Martina et al. 2000; Stuart et al. 1997a; Turner et al. 1991), and the spread of these dendritic APs toward the soma is known as forward propagation. Understanding the factors that determine the efficacy of AP propagation in dendrites is important since AP propagation has key consequences for the integration of synaptic input and the induction of synaptic plasticity (Johnston et al. 1996; Linden 1999). In particular, backpropagation of the AP provides a mechanism whereby information about neuronal output is signaled backward to active synapses to trigger changes in synaptic strength (Linden 1999; Stuart et al. 1997b).

A striking finding that has emerged from recent studies is that under similar experimental conditions, systematic differences in backpropagation exist between neuronal types (reviewed by Stuart et al. 1997b). In dopamine neurons (Häusser et al. 1995) and mitral cells (Bischofberger and Jonas 1997; Chen et al. 1997), the somatic AP propagates nondecrementally to the distal dendrites. On the other hand, many neuronal types show decremental conduction, with the most extreme example being cerebellar Purkinje cells, where the AP is reduced to a few millivolts in amplitude at 100 μm from the soma (Llinás and Sugimori 1980; Stuart and Häusser 1994). A comparable diversity has also been observed for the efficacy of forward propagation of dendritically initiated APs toward the soma (Chen et al. 1997; Golding and Spruston 1998; Kamondi et al. 1998; Llinás and Sugimori 1980; Martina et al. 2000; Schwindt and Crill 1998; Stuart et al. 1997a).

Explanations for these systematic differences in the efficacy of propagation have concentrated on differences in the densities of dendritic voltage-gated channels (Magee et al. 1998; Stuart et al. 1997b). Theoretical work on AP propagation in axons has demonstrated that propagation is dependent on axonal morphology (Goldstein and Rall 1974; Joyner et al. 1980; Lüscher and Shiner 1990; Manor et al. 1991; Parnas and Segev 1979; Ramon et al. 1975). The wide variety of dendritic arborizations among different neuronal types suggests that differences in dendritic morphology will contribute to determining the extent of backpropagation and forward propagation of APs in dendrites. This is a difficult issue to address quantita-

---

tively as cable theory does not provide an analytical solution describing action potential propagation in arbitrarily branched cable structures and systematic experimental manipulations of dendritic morphology are not yet possible. We have therefore examined this question with simulations of AP propagation in a wide range of realistic dendritic geometries. By inserting the same set of passive and active parameters in each cell type, we have isolated the effect of geometry alone (Mainen and Sejnowski 1996). We show that dendritic geometry plays a key role in determining the efficacy of both forward and backward propagation of APs. These results have important implications for modulation of backpropagation and for the role of the dendritic AP as an associative signal in different neurons.

METHODS

Dendritic geometries

Detailed three-dimensional reconstructions of 42 neurons were used. Two rat Purkinje cells, two rat neocortical layer 5 pyramidal neurons, and four rat substantia nigra dopamine neurons were filled with biocytin and digitally reconstructed using a ×100 oil immersion objective (1.4 NA) on a Zeiss Axioplan (Zeiss, Oberkochen, Germany) in conjunction with Neurolucida software (MicroBrightField, Colchester, VT). Three rat layer 5 pyramidal neurons were from G. Stuart and N. Spruston, and one from D. Smetters; three guinea pig Purkinje cells were from M. Rapp; rat CA1/CA3 pyramidal cells, and DG interneurons and granule cells were obtained from the Duke-Southampton Neuronal Morphology Archive (www.neuro.soton.ac.uk). Reconstructions were inspected carefully, and only those without apparent errors in connectivity or dendritic diameters were used. All dendrites were divided into compartments with a maximum length of 7 μm. Spines were incorporated where appropriate by scaling membrane capacitance and conductances (Holmes 1989; Shelton 1985).

Simulations

Simulations were performed using the NEURON simulation environment (Hines and Carnevale 1997) on a Pentium II PC running Red Hat Linux and on a Silicon Graphics Origin 2000. The time step for the simulations was 25 μs. The structure of the active model was based on recent modeling studies (Mainen and Sejnowski 1996; Mainen et al. 1995; Rapp et al. 1996). Two Hodgkin–Huxley-type conductances (g_{Na} and g_{K}) were inserted into the soma, dendrites, and spines at uniform densities. For simplicity, we did not explore the consequences of using spines with different excitability from dendritic shafts (see Baer and Rinzel 1991). The model was tuned by attaching a synthetic axon (Mainen et al. 1995) to five neocortical pyramidal cell geometries in which backpropagating APs were initiated by somatic current injection. Active and passive membrane parameters were then optimized to reproduce experimental data on AP backpropagation from these neurons in slices taken from rats aged P26–30 (Stuart et al. 1997a). The uniform passive parameters of the model were R_{i} = 150 Ωcm, C_{m} = 1 μF/cm^2, R_{m} = 12 kΩcm^2, which reproduced experimental values for membrane time constant and input resistance to within 10% (Stuart and Spruston 1998; Stuart et al. 1997a). The standard values for g_{Na} and g_{K} were 35 and 30 pS/μm^2, respectively, and the channel models were identical to those used by Mainen and Sejnowski (1996) (available from www.cnl.salk.edu/simulations/). Channel kinetics and densities were adjusted for a nominal temperature of 37°C using a Q_{10} of 2.3. All results shown in the figures and tables were obtained using this standard model. In some cases, the standard g_{Na} and g_{K} were replaced by corresponding channel models from a different study (Paré et al. 1998). Simulations using a nonuniform distribution of the A-type K$^+$ channel were based on previous studies (Hoffman et al. 1997; Migliore et al. 1999). The A-type K$^+$ channel replaced the K$^+$ channel used in the standard model, and its density was scaled to increase linearly fivefold from the soma to the most distal dendrites of each neuron, with the initial density being 480 pS/μm^2 (Hoffman et al. 1997; Migliore et al. 1999).

The morphology of the soma and proximal dendrites may itself affect the invasion of the soma by the axonally initiated AP. Therefore a somatic AP waveform (amplitude, 96 mV; half-width, 0.6 ms) obtained from one of the pyramidal neuron morphologies with the standard model was used as a voltage-clamp command at the soma of all other neurons to simulate backpropagation. This ensured a fair comparison across all neurons so that backpropagation begins from the same initial conditions in each morphology (simulations with a synthetic axon attached to all morphologies, allowing each to generate its own AP, produced very similar results). The dendritically initiated AP was generated using a biexponential synaptic conductance (τ_{rise} = 0.2 ms, τ_{dec} = 1.7 ms, g_{max} = 50 nS) near the apical nexus of a neocortical pyramidal cell (622 μm from the soma; see Fig. 6). This waveform was used as a voltage-clamp command to examine propagation of a dendritic AP, again to ensure that propagation begins from the same initial conditions. In this way, AP propagation was isolated from AP initiation, conditions for which also depend on morphology (Segev and Rall 1998). Similar results were obtained using a somatic AP waveform, or a backpropagating dendritic AP waveform.

Measurements

The rate of increase of membrane area as a function of distance from the soma (dA/dx) was approximated by $\Delta A/\Delta x$, where ΔA is the spine-adjusted total membrane area at a distance interval (x, $x + \Delta x$) from the soma. The discretization Δx was 1 μm (Δx = 0.25 μm for Purkinje cells). All distances were measured along the dendrites. The somatodendritic Na$^+$ channel density threshold for full AP propagation into all dendritic branches, $g_{Na,thresh}$, was determined using the bisection algorithm (Press et al. 1992). The radius of equivalent cables was calculated according to the following equation

$$r_{eq}(X) = \left(\sum_{j} r_{j}(X)^{3/2} \right)^{2/3} \qquad (1)$$

where the sum is over all dendritic segments j located at a given electrotonic distance X from the soma (Clements and Redman 1989; Fleshman et al. 1988; Ohme and Schierwagen 1998), with discretization ΔX = 0.004. Impedance mismatch at a given point in a morphology was calculated by splitting the morphology into two subtrees at that point and measuring the input impedances (200 Hz) of the two individual subtrees. Input impedances were calculated using the standard values of the passive parameters and g_{Na} and g_{K}. The impedance mismatch was then calculated as the ratio of the input impedance of the subtree where the AP originated over the input impedance of the subtree that the AP is propagating into. Correlations were assessed using the Pearson correlation coefficient r; correlations mentioned in the text and shown in the figures are highly significant ($P < 0.001$). Values are given as means $\pm$ SE. All scripts for simulations and measurements are available from the authors or from www.dendrites.org.

RESULTS

Backpropagation depends on dendritic geometry

We designed a simple active model to reproduce experimental data on AP backpropagation in a single cell type to then apply it to a range of different morphologies. We used a model of neocortical pyramidal cells since extensive data on backpropagation are available for this cell type. Furthermore these neurons fall in the middle of the range of backpropagation

efficacies (Stuart et al. 1997b). The model was based on previous studies (Mainen and Sejnowski 1996; Mainen et al. 1995; Rapp et al. 1996) and incorporated a uniform density of Na^+ and K^+ channels in the soma and dendrites with a high density of Na^+ channels in the axon to ensure axonal initiation of the AP. This simple model is able to reproduce the experimental data in neocortical pyramidal cells remarkably well (cf. Figs. 1B and 2A of Stuart et al. 1997a).

To isolate the effect of dendritic morphology, the same model was then inserted into morphologies of different cell types, and backpropagation of a somatic AP waveform was simulated. With identical channel types and densities, the different morphologies produced very different patterns of backpropagation (Fig. 1), which reproduced the experimentally observed results in these neurons (Häusser et al. 1995; Llinás and Sugimori 1980; Stuart and Häusser 1994; Stuart and Sakmann 1994; Stuart et al. 1997a). Thus the AP spread effectively into all dendritic branches of substantia nigra dopamine neurons while propagating decrementally in the apical dendrite of neocortical pyramidal cells and failing to effectively invade the dendritic tree of Purkinje cells. Interestingly, even within the same neuron a wide range of AP amplitudes could be observed
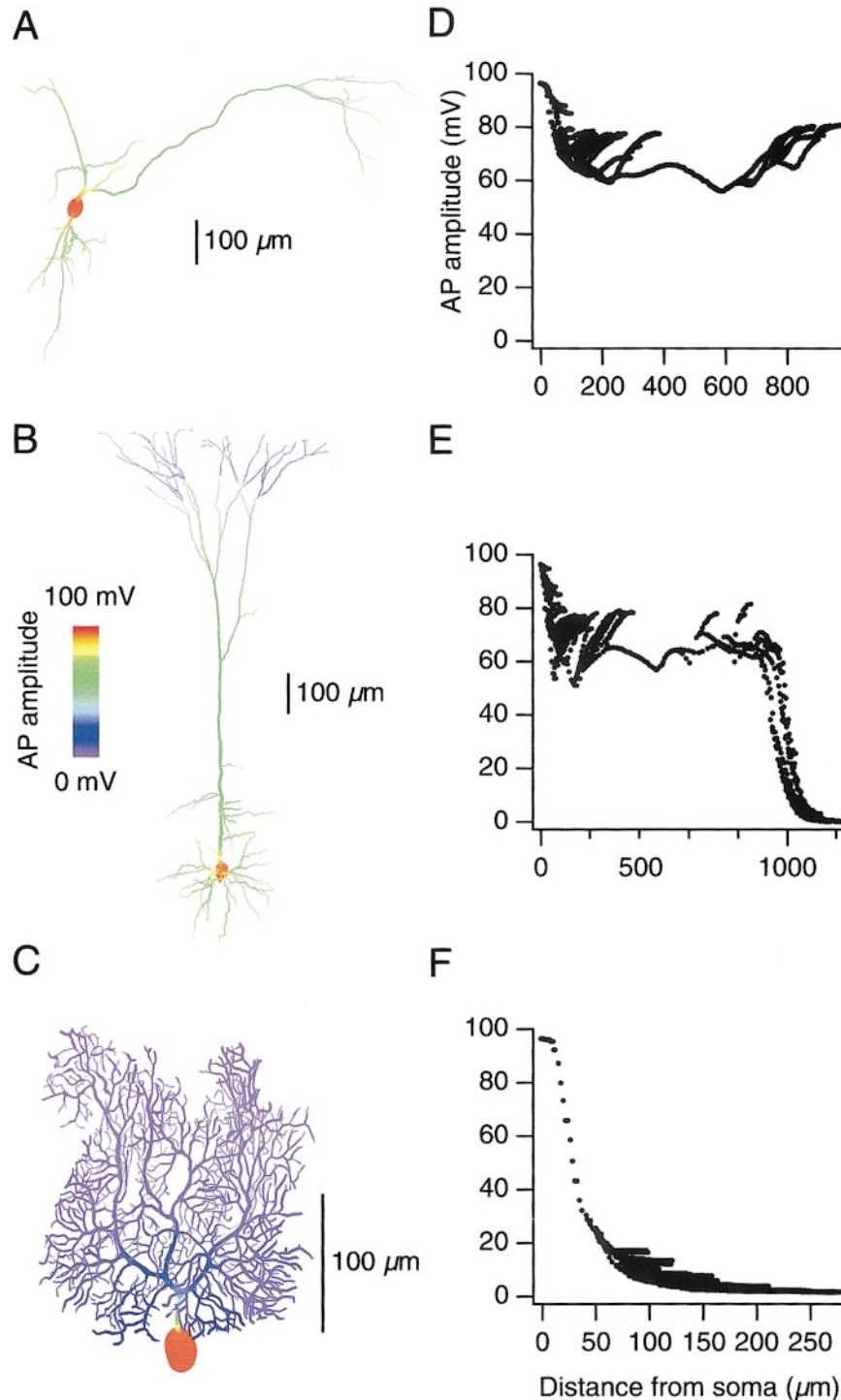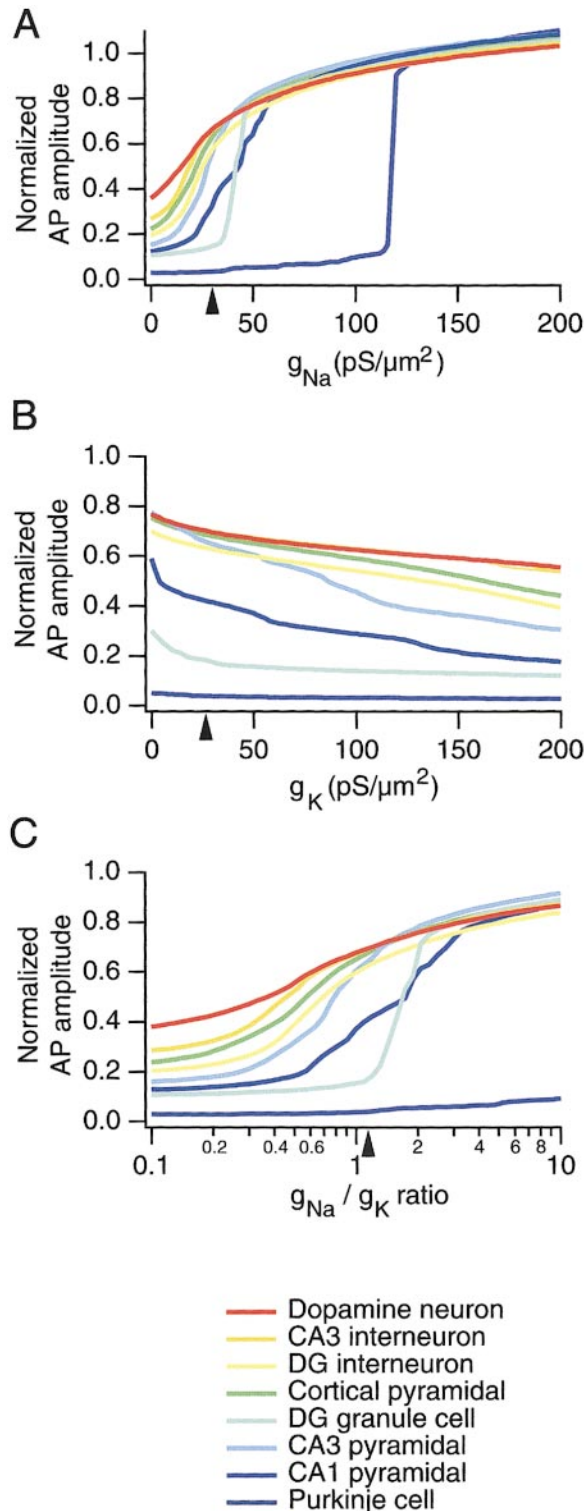

FIG. 1. Backpropagation of action potentials (APs) in different morphologies with identical channel types and distributions. *A–C*: 2-dimensional projections of 3-dimensional digital reconstructions of a substantia nigra dopamine neuron (*A*), a neocortical layer 5 pyramidal cell (*B*), and a cerebellar Purkinje cell (*C*). The local amplitude of a backpropagating AP elicited by voltage-clamping the soma with a standard somatic AP waveform is coded by color. *D–F*: scatter plots of dendritic AP amplitude vs. distance from the soma for the cells shown in *A–C*. Each point represents the peak AP amplitude in each dendritic compartment.

at the same physical distances from the soma (Fig. 1E). As the density of Na^+ and K^+ channels is uniform in this model, the diversity in propagation into different dendritic branches must be a consequence of the morphology. Taken together, these findings indicate that dendritic geometry determines the interaction between a given Na^+ channel density and backpropagation.

FIG. 2. Sensitivity of backpropagation to voltage-gated channel density in different cell types. *A*: effect of varying Na^+ channel density on backpropagation. The results of simulations in 8 representative neurons from different cell types are shown with cell type coded by color (legend at *bottom*). The average dendritic AP amplitude at 200 μm from the soma (normalized by the somatic AP amplitude) is plotted vs. somatodendritic Na^+ channel density. Somatodendritic K^+ channel density was kept fixed at 30 pS/μm^2. ▲, the Na^+ channel density used in the standard model (see METHODS). *B*: effect of varying K^+ channel density. Simulations as in *A*, except somatodendritic K^+ channel density was varied while keeping Na^+ channel density constant at 35 pS/μm^2. ▲, the K^+ channel density used in the standard model. *C*: effect of varying the relative density of Na^+ and K^+ channels. Simulations as in *A*, except the ratio of somatodendritic K^+ and Na^+ channel density was varied, while keeping the sum of the channel densities constant at 65 pS/μm^2. ▲, the channel density ratio used in the standard model.

Sensitivity of backpropagation to channel density in different morphologies

To investigate the relationship between backpropagation and voltage-gated channel density in different morphologies, we simulated backpropagation over a wide range of Na^+ and K^+ channel densities (from 0 to 200 pS/μm^2). These simulations were carried out in a large sample of different neuronal types, including the neurons studied in the preceding text as well as hippocampal CA1 and CA3 pyramidal neurons, dentate gyrus (DG) granule cells, and hippocampal interneurons. First, we varied the Na^+ channel density while keeping the K^+ channel density constant. Each neuronal type had a characteristic relation between dendritic Na^+ channel density and backpropagation (quantified by measuring the AP amplitude 200 μm from the soma; Fig. 2A). With no dendritic Na^+ channels, the attenuation of the AP waveform was very different in different neuronal types (see Table 1). This indicates that the dendritic morphologies filter the AP waveform to different extents even when backpropagation is passive. When Na^+ channel density was increased, an approximately sigmoid relationship was observed between density and propagation efficacy in most cell types. The half-maximum of these curves was typically around 20–40 pS/μm^2 (see Table 1), within the physiological range of dendritic Na^+ channel densities (Johnston et al. 1996). In striking contrast, backpropagation in Purkinje cells was essentially insensitive to increases in Na^+ channel density over a wide range with a sharp threshold leading to full backpropagation being reached only at very high densities (mean half-maximum, 92.8 ± 23.3 pS/μm^2).

We next varied the density of dendritic K^+ channels while maintaining a constant Na^+ channel density. As expected, when K^+ channel density was increased, backpropagation became less effective. Although backpropagation was less sensitive to changes in dendritic K^+ channel density than changes in Na^+ channel density, there was a characteristic relationship between K^+ channel density and backpropagation in each neuronal type (Fig. 2B). Over the range studied (from 0 to 200 pS/μm^2), backpropagation in Purkinje cells and dopamine neurons showed little sensitivity to changes in K^+ channel density, while backpropagation in pyramidal neurons and dentate gyrus granule cells was clearly affected (Fig. 2B).

In the same set of neurons, we also examined the sensitivity of backpropagation to changes in the *relative* densities of dendritic Na^+ and K^+ channels. This was done by systematically varying the ratio of densities over a wide range (0.1–10) while keeping the total voltage-gated channel density fixed. As shown in Fig. 2C, most neurons showed a sigmoid relationship

TABLE 1. *Dependence of AP backpropagation on voltage-gated channel density in different neuronal types*

Cell Type	n	Passive AP Backpropagation Ratio*	Half-Maximal g_{Na}, pS/μm^2†	Half-Maximal g_{Na}/g_K Ratio‡
Purkinje cell	5	0.06 ± 0.01	92.8 ± 23.3	2.15 ± 0.41
CA1 pyramidal cell	4	0.14 ± 0.01	37.7 ± 2.6	1.30 ± 0.18
CA3 pyramidal cell	5	0.16 ± 0.01	31.6 ± 1.8	0.97 ± 0.04
DG granule cell	6	0.14 ± 0.02	33.5 ± 2.1	1.11 ± 0.15
Cortical pyramidal cell	7	0.21 ± 0.01	21.4 ± 2.6	0.68 ± 0.05
DG interneuron	6	0.25 ± 0.03	22.4 ± 1.5	0.72 ± 0.06
CA3 interneuron	5	0.30 ± 0.03	20.9 ± 3.1	0.74 ± 0.10
Dopamine neuron	4	0.27 ± 0.04	19.2 ± 1.2	0.64 ± 0.03

Values are means $\pm$ SE. * Amplitude of dendritic action potential (AP) 200 μm from the soma, normalized by somatic AP amplitude, with zero g_{Na} (conditions as in Fig. 2A). † Density of somatodendritic Na$^+$ channels at which half-maximal AP backpropagation occurs (conditions as in Fig. 2A). ‡ Ratio of g_{Na}/g_K at which half-maximal AP backpropagation occurs (conditions as in Fig. 2C).

with backpropagation efficacy as the density of Na$^+$ channels relative to K$^+$ channels was increased. However, the half-maximum of the curve depended strongly on morphology and spanned a wide range (Table 1). Again Purkinje cells were particularly insensitive to changes in dendritic channel densities. These findings demonstrate that, as expected, backpropagation depends on the relative density of dendritic voltage-gated Na$^+$ and K$^+$ channels. However, the same ratio of channel densities produces very different degrees of backpropagation in different morphologies. Furthermore the effect of changing the relative density depends critically on the dendritic morphology.

On the basis of these simulations, we defined an index of backpropagation that reflects the different sensitivities of the morphologies to channel densities. As backpropagation is most sensitive to Na$^+$ channel density, we determined the minimum Na$^+$ channel density required for full backpropagation of the AP (peak voltage >0 mV) into all dendritic branches. The threshold Na$^+$ channel density ($g_{Na,thresh}$) varied widely across cell types (Fig. 3). Purkinje cells required nearly five times higher Na$^+$ channel density than dopamine neurons to sustain full backpropagation into all dendrites. We therefore used $g_{Na,thresh}$ as a measure that captures the efficacy of propagation in a given neuron.

Morphological determinants of backpropagation

Which morphological features are most important for determining the efficacy of backpropagation? Unfortunately no analytical theory exists to predict whether propagation will be successful given a dendritic morphology and a set of realistic channel densities and kinetics (Jack et al. 1983). Attempts to formulate such a theory have so far succeeded only for simple geometries, using highly simplified models of excitability (Pastushenko et al. 1969; Pauwelussen 1982). We therefore examined correlations of individual geometric parameters with our functional index of backpropagation, $g_{Na,thresh}$, and with the amplitude of the AP 200 μm from the soma (AP$_{200}$) using the standard parameters of the model. The simplest morphological features, such as mean dendritic diameter, total physical or electrotonic length of the dendrites, dendritic taper or flare, and total dendritic membrane area only correlated relatively weakly with $g_{Na,thresh}$ or AP$_{200}$ ($|r| \leq 0.6$). The number of dendritic branchpoints, however, showed a strong relationship with the functional parameters across the population (Fig. 4A; $r = 0.81$ and -0.73 for $g_{Na,thresh}$ and AP$_{200}$, respectively). The range of

branching densities was reflected in striking differences in the distribution of dendritic membrane area with distance x from the soma (dA/dx, Fig. 4B). Both $g_{Na,thresh}$ and AP$_{200}$ were strongly correlated with the maximum slope of dA/dx across the different morphologies (Fig. 4C). Combining features of the dA/dx distribution with another geometric parameter (e.g., the maximum slope normalized to the number of branchpoints or mean dendritic diameter) further strengthened correlations with $g_{Na,thresh}$ and AP$_{200}$, such that correlation coefficients of $|r| > 0.9$ were obtained.

We tested the robustness of these correlations in several ways. First, each of the passive parameters were changed over a wide range (R_i: 70–200 Ωcm, C_m: 0.7–1.5 μF/cm^2, R_m: 5–50 kΩcm^2). Second, different models for the Hodgkin-Huxley g_{Na} and g_K conductances (taken from Paré et al. 1998) were incorporated. The qualitative behavior of the models remained robust under these different conditions, as did the ranking of correlations between morphology and backpropagation; values of individual correlations varied by less than 20%. Finally, as a nonuniform distribution of A-type K$^+$ channels has recently been demonstrated to play an important role in regulating backpropagation in hippocampal pyramidal neurons (Hoffman et al. 1997) and mitral cells (Schoppa and Westbrook 1999),
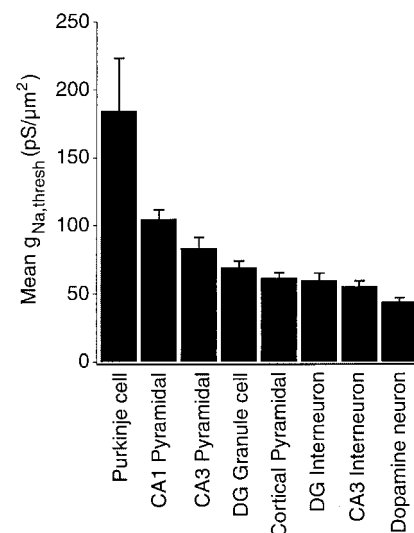
FIG. 3. Cell-specific dependence of backpropagation on Na$^+$ channel density. Bar chart of the minimum somatodendritic Na$^+$ channel density required for full AP backpropagation (>0 mV) into all dendritic branches in different neuronal types. Each cell type is represented by at least 4 morphologies.
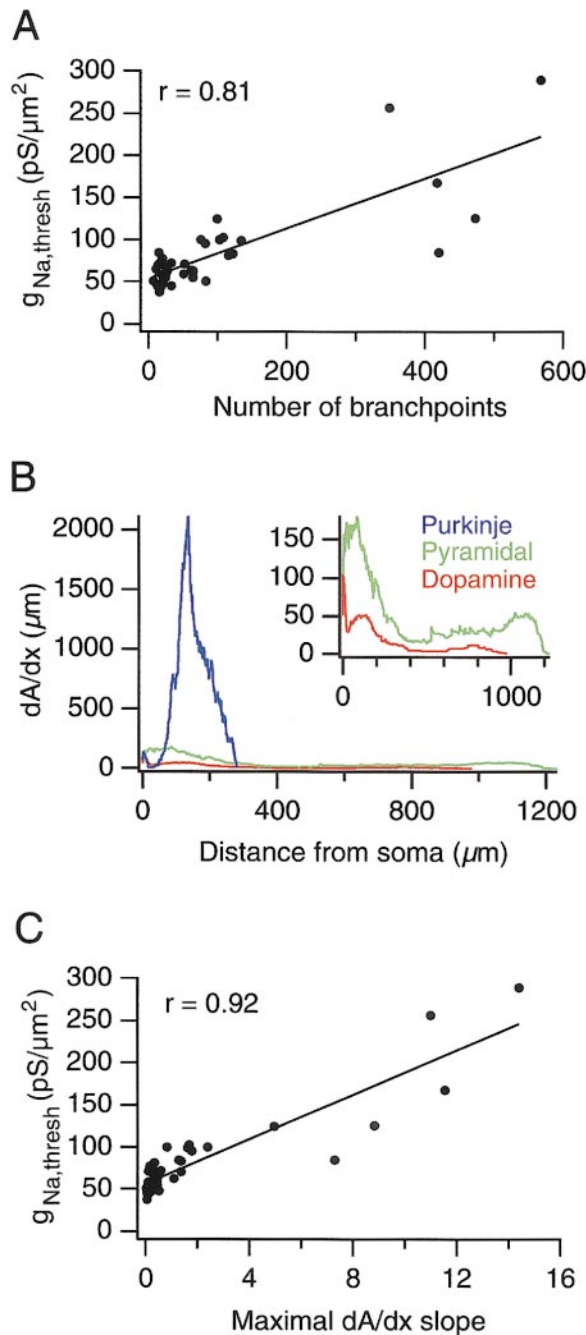
FIG. 4. Morphological determinants of backpropagation. *A*: relationship between the number of dendritic branchpoints and $g_{Na,thresh}$. Each point represents 1 neuron ($n = 42$ neurons). *B*: rate of increase in membrane area with distance from the soma (dA/dx) in a nigral dopamine neuron (red), a neocortical pyramidal cell (green), and a Purkinje cell (blue); same cells as in Figs. 1 and 2. *Inset*: the data for the pyramidal cell and the dopamine cell on an expanded axis. *C*: relationship between the maximum slope of the smoothed dA/dx distribution and $g_{Na,thresh}$.

used to estimate the relative efficacy of backpropagation in a given dendritic morphology.

Which measure provides the best functional link between the details of dendritic morphology and backpropagation efficacy? Simulations of AP propagation in axons (Goldstein and Rall 1974; Lüscher and Shiner 1990; Manor et al. 1991) have shown that propagation across a branchpoint depends on the ratio of the input impedances of the parent and daughter branches—the impedance mismatch (Goldstein and Rall 1974). If this ratio equals one, there is no change in propaga-
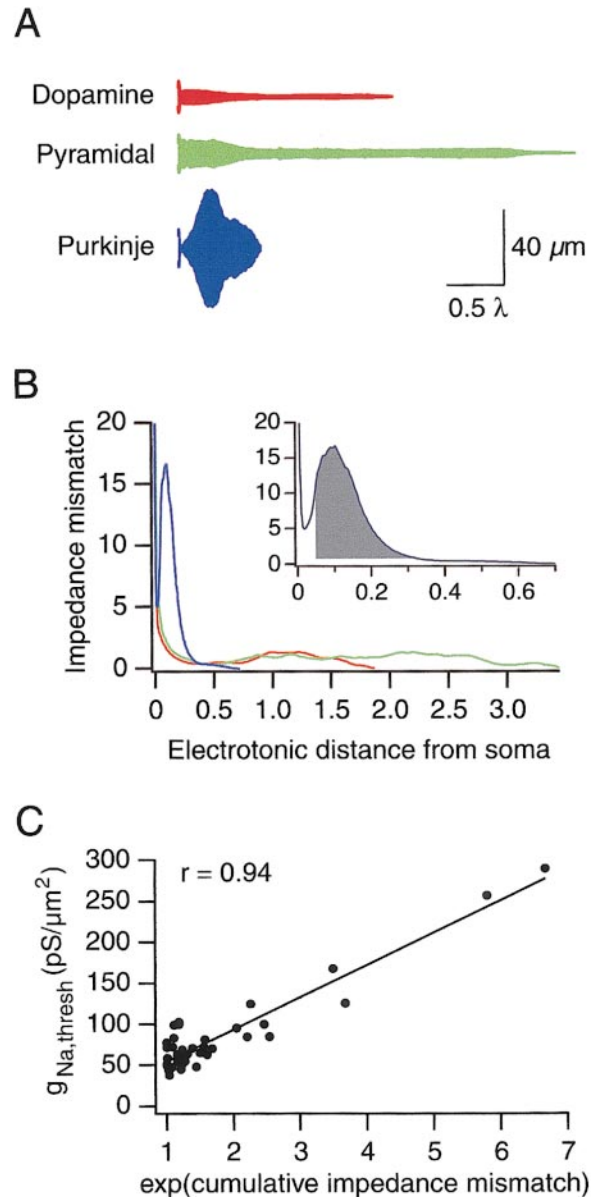

FIG. 5. A reduced model of dendritic geometry predicts the efficacy of backpropagation. *A*: profiles of equivalent cables constructed from the cells shown in Fig. 1. The vertical axis corresponds to the radius of the equivalent cable, and the horizontal axis to the electrotonic distance (λ, electrotonic space constant). *B*: impedance mismatch as a function of electrotonic distance from the soma for the equivalent cables shown in *A*. The cumulative impedance mismatch is defined by the area shown for the Purkinje cell in the *inset* (integral bounded by $X = 0.05$ on the *left* to exclude the soma, and an impedance mismatch of 1.0 at the *bottom*). *C*: relationship between the cumulative impedance mismatch in the equivalent cable (scaled exponentially) and $g_{Na,thresh}$ in the respective original morphology.

we incorporated a nonuniform distribution of an A-type K+ channel model (Migliore et al. 1999) into the simulations based on experimental and modeling studies (Hoffman et al. 1997; Migliore et al. 1999). Even with this nonuniform channel distribution, strong correlations were observed between dendritic morphology and backpropagation (e.g., $r = 0.91$ for $g_{Na,thresh}$ and the maximum slope of dA/dx). Taken together, these findings suggest that geometric parameters alone can be
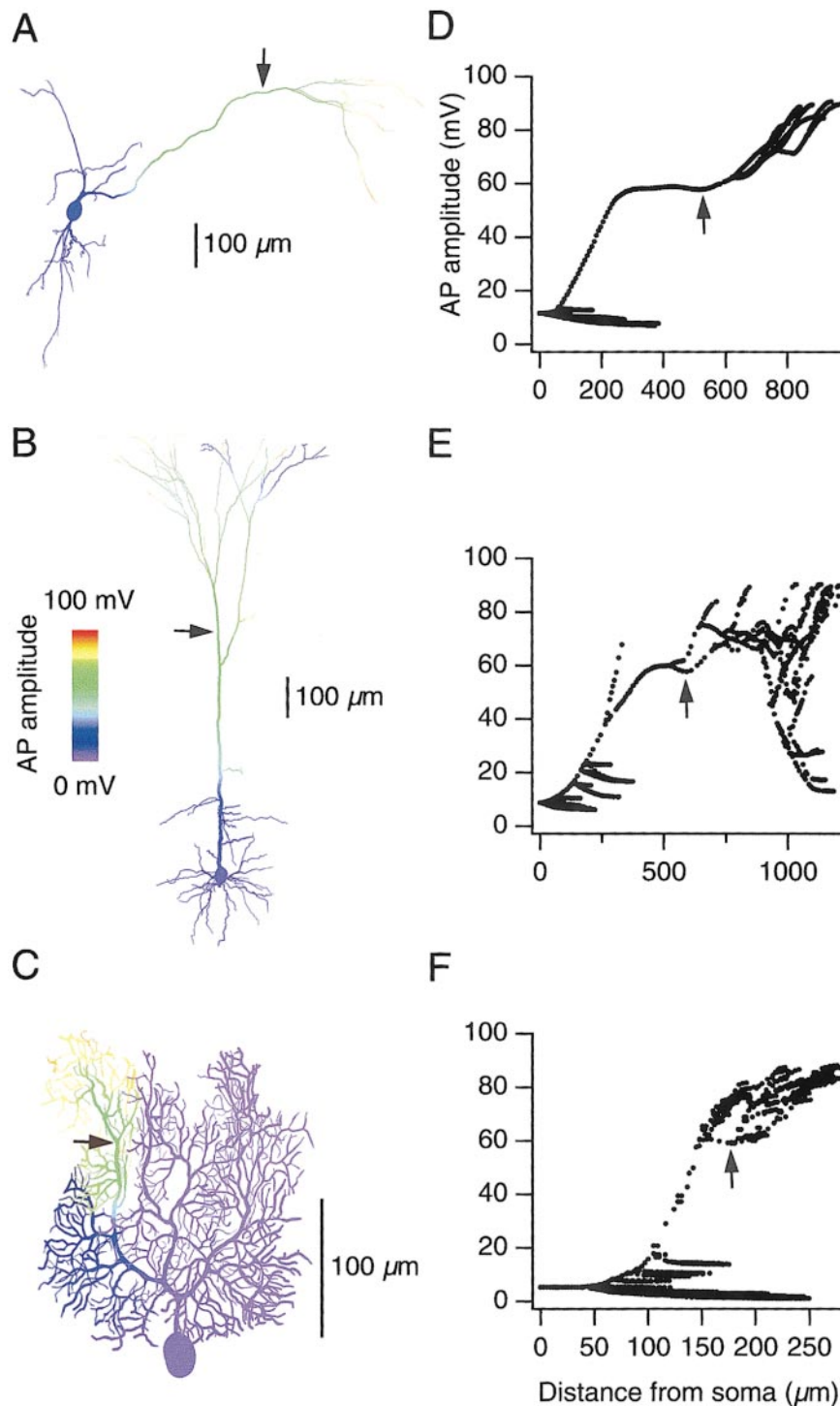
FIG. 6. Forward propagation of dendritically initiated APs. *A–C*: a dendritic AP was initiated in the neocortical pyramidal cell (*B*) using a synapse located at →. The propagation of this AP in a nigral dopamine neuron (*A*) and a cerebellar Purkinje cell (*C*) was examined by applying it as a voltage-clamp command at the location indicated (→). The local amplitude of the propagating dendritic AP is coded by color. Propagation into the distal dendrites differs from that shown in Fig. 1 because the waveform of the dendritically initiated AP at its site of generation differs from the waveform of the backpropagating AP at the same site. *D–F*: scatter plots of dendritic AP amplitude vs. distance from the soma for the cells shown in *A–C*.

tion of the AP as it approaches the branchpoint. However, if it is greater than one, i.e., if the combined input impedance of the daughter branches is lower than the input impedance of the parent branch, AP propagation may fail. For branches of uniform diameter and semi-infinite length, the impedance mismatch is given by Rall's geometric ratio (GR)

$$GR = \sum_d r_d^{3/2}/r_p^{3/2} \qquad (2)$$

where r_d are the radii of the daughter branches and r_p is the radius of the parent branch. As the mean GR for all dendritic branchpoints in each of our morphologies was 2.4 ± 0.08 ($n = 42$), this may explain the relatively strong correlation of $g_{Na,thresh}$ with the number of branchpoints (Fig. 4*A*).

However, dendritic branches in realistic dendritic trees are finite in length, and the branchpoints are not the only sites contributing to the impedance mismatch along a dendrite. Usually a succession of several branchpoints, connected by sections with taper or flare, lies within the spatial extent of a dendritic AP. Thus it is difficult to predict the relative importance of various local maxima in the impedance mismatch in determining the fate of the AP except by explicit simulation of
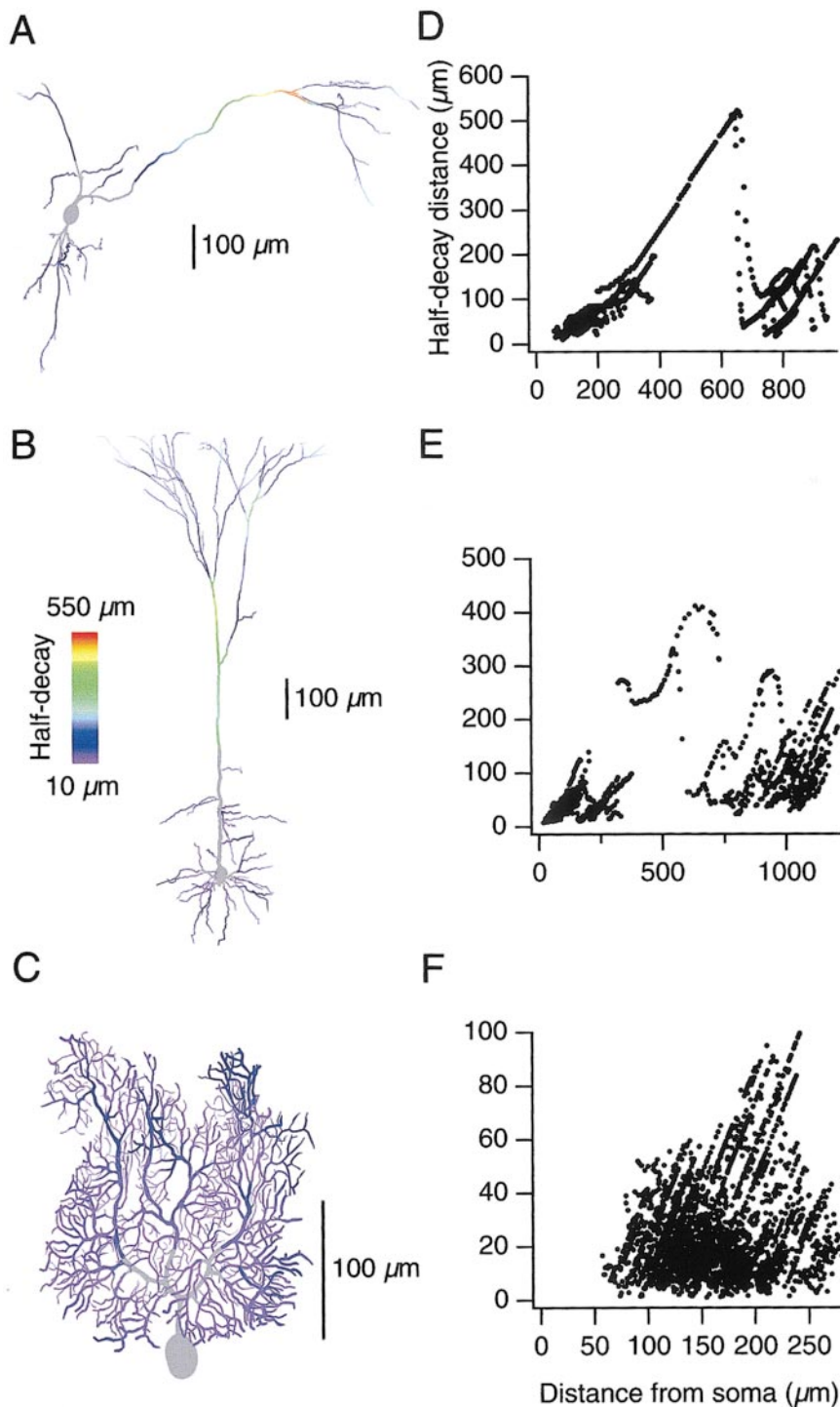
FIG. 7. Forward propagation depends on dendritic geometry. *A–C*: forward propagation of a dendritic AP was simulated successively at all dendritic locations in a nigral dopamine neuron (*A*), a layer 5 pyramidal cell (*B*), and a cerebellar Purkinje neuron (*C*). For each dendritic location, the distance at which the amplitude of the forward propagating dendritic AP was reduced to half of its amplitude was measured. This "half-decay" distance is coded by color at the site of origin. For some input regions (i.e., those at or close to the soma), the AP never decays to half of its amplitude before reaching the soma. These regions are indicated in gray. The same data are plotted in *D–F* as a scatter plot showing the half-decay distance of the dendritic AP initiated at a given location versus distance of that location from the soma.

AP propagation (Figs. 1–3) (Lüscher and Shiner 1990; Manor et al. 1991). To obtain a better predictor of AP propagation, we simplified the analysis of impedance mismatches by constructing reduced models of the dendritic architecture (Segev 1992), transforming each dendritic morphology into a single unbranched equivalent cable (Fig. 5*A*) (Clements and Redman 1989; Fleshman et al. 1988; Ohme and Schierwagen 1998). The impedance mismatch calculated in this cable approximates the mean impedance mismatch seen by an AP wavefront propagating in the original dendritic morphology. The shape of the impedance mismatch distribution (Fig. 5*B*) proved to be closely related to the efficacy of backpropagation. In particular, the cumulative impedance mismatch (Fig. 5*B, inset*) is a remarkably good predictor of both $g_{Na,thresh}$ ($r = 0.94$; Fig. 5*C*) and AP_{200} ($r = -0.89$).

Forward propagation of dendritic APs depends on dendritic geometry

Under some circumstances, it is possible to initiate Na^+ APs in dendrites. These dendritic APs propagate with variable efficacy to the soma in different cell types (Chen et al. 1997;

Golding and Spruston 1998; Kamondi et al. 1998; Martina et al. 2000; Schwindt and Crill 1998; Stuart et al. 1997a). We investigated the influence of morphology on the extent of this forward propagation by comparing propagation of a dendritic AP in our set of neurons. The same dendritic AP waveform propagated to very different extents in different neurons with an identical distribution of voltage-gated channels (Fig. 6). In dopamine neurons and pyramidal neurons, propagation of the dendritic AP was very effective, while in Purkinje cells the dendritic AP was rapidly attenuated.

The spread of a dendritic AP is likely to depend on its site of origin in the dendritic morphology, as previously shown for spread of signals in passive dendrites (Rall 1964; Zador et al. 1995). We therefore systematically examined the spread of the dendritic AP from all locations in each dendritic tree. To quantify the extent of forward propagation, we measured the distance at which the dendritic AP was reduced to half its original amplitude when traveling toward the soma. This "half-decay distance" depended strongly on the site of origin of the dendritic AP and on the cell type (Fig. 7). The dendritic AP could propagate for hundreds of micrometers toward the soma from many dendritic locations in both dopamine and neocortical pyramidal neurons. In contrast, for nearly all locations in the cerebellar Purkinje cell, propagation was limited to less than 50 μm, being restricted to the branchlets close to the initiation site. As shown in Table 2, the mean half-decay distance of the dendritic AP calculated over all sites of origin depended strongly on cell type. These findings indicate that the local geometry as well as the overall structure of the dendritic tree are important determinants of forward propagation of dendritic APs.

To examine the relationship between dendritic Na$^+$ channel density and forward propagation, we determined $g_{Na,thresh}$ (this time defined as the threshold g_{Na} for full propagation to the soma) for forward propagating APs. As for backpropagation, $g_{Na,thresh}$ depended on cell type (Fig. 8A), with Purkinje cells again requiring the highest density of Na$^+$ channels to ensure full propagation. The sequence of propagation efficacies was slightly different from that observed for backpropagation, consistent with the asymmetry of the dendritic architecture. To determine if the underlying principles established for back-propagation also hold for propagation in the forward direction,

TABLE 2. *Extent of forward propagation of a dendritically initiated AP in different neurons*

Cell Type*	Mean Half-Decay Distance, μm†	Maximal Half-Decay Distance, μm‡
Purkinje cell	29 ± 3	113 ± 12
CA1 pyramidal cell	85 ± 5	323 ± 58
CA3 pyramidal cell	138 ± 12	709 ± 116
DG granule cell	128 ± 10	296 ± 22
Cortical pyramidal cell	80 ± 6	447 ± 75
DG interneuron	99 ± 10	268 ± 22
CA3 interneuron	130 ± 12	377 ± 29
Dopamine neuron	143 ± 16	514 ± 83

Values are means ± SE. * Same cells as in Table 1. † Mean distance at which the dendritic AP is reduced to half its original amplitude during propagation to the soma for all sites of origin in the morphology (conditions as in Fig. 7). Input regions from which the dendritic AP did not decay to half of its amplitude were excluded from the average. ‡ As in †, except the maximal distance measured is given.
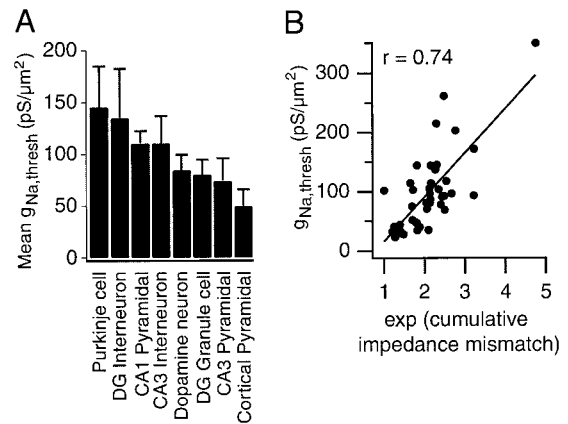

FIG. 8. Morphological determinants of forward propagation. *A*: bar chart of the minimum somatodendritic Na$^+$ channel density required for full AP propagation to the soma in different neuronal types. The origin of the dendritic AP was 200 μm from the soma on the longest dendritic path. Same morphologies as in Fig. 3. *B*: correlation between the cumulative impedance mismatch (scaled exponentially and measured as in Fig. 5*B*) in the equivalent cable constructed from the point of origin of the dendritic AP and $g_{Na,thresh}$ for forward propagation in the respective original morphology (n = 42 neurons).

we constructed equivalent cables from the point of view of the origin of the dendritic AP. Again the cumulative impedance mismatch in the equivalent cable was an accurate predictor of propagation efficacy (Fig. 8*B*). Thus as for backpropagation, a reduced model of dendritic geometry (Segev 1992) is able to provide a tight functional link between morphology and the efficacy of forward propagation.

DISCUSSION

We have shown that dendritic morphology plays an important role in determining both forward propagation and back-propagation of APs in dendrites. Recent work has highlighted the importance of dendritic voltage-gated channels in regulating the efficacy of AP propagation. Our findings complement this work and demonstrate that morphological features act in concert with dendritic voltage-gated channels to generate the observed diversity of AP propagation in dendritic trees of different neuronal types. Although there are clear differences in channel densities and properties between neurons (Johnston et al. 1996; Llinás 1988), we show that dendritic geometry determines how significant these differences are for neuronal function. These findings have important consequences for our understanding of how different neurons use dendritic APs as computational signals.

The link between dendritic morphology and propagation

Our findings demonstrate that some dendritic morphologies are remarkably resistant to AP propagation. Purkinje cells, for example, do not show effective propagation even with relatively high densities of voltage-gated Na$^+$ channels. This indicates that, as predicted by Rall (1964), the poor AP back-propagation observed experimentally in Purkinje cells is primarily due to their distinctive morphology in conjunction with the relatively low channel densities (Stuart and Häusser 1994) and narrow AP widths (Stuart et al. 1997b) found in these neurons. On the other hand, we have also identified dendritic geometries—such as those of dopamine neurons—

that are very favorable for propagation, requiring only very low Na^+ channel densities for effective propagation into the distal dendrites. These findings suggest that the diversity in back-propagation efficacy observed experimentally (Stuart et al. 1997b) may be a consequence of the diversity in dendritic morphologies in different neurons. As forward propagation is also influenced by dendritic geometry in a similar manner, we predict that the experimentally observed differences in forward propagation may also result in part from differences in dendritic structure. Although our simulations have focused on APs mediated by Na^+ channels, it is likely that propagation of dendritic calcium spikes (Amitai et al. 1993; Helmchen et al. 1999; Kim and Connors 1993; Larkum et al. 1999b; Llinás and Sugimori 1980; Schiller et al. 1997; Schwindt and Crill 1998; Seamans et al. 1997; Yuste et al. 1994) is also regulated by morphology over a wide range.

By correlating morphological features with AP propagation, we have shown that the number of dendritic branchpoints is a critical variable for determining propagation efficacy. An even more accurate predictor of propagation efficacy is the rate of increase in dendritic membrane area, which is determined by the number of branchpoints and the relationship between the diameter of parent and daughter dendrites at branchpoints. Based on this strong correlation, we can make predictions about the relative efficacy of propagation for several cell types in which propagation has not been measured directly (e.g., granule cells and interneurons in the dentate gyrus). This measure should also permit similar predictions to be made for any dendritic morphology.

The link between the distribution of membrane area and propagation can be understood by noting that the functions describing the rate of increase in membrane area and the radius of the equivalent cable are closely related. For real dendrites, this leads to distributions of similar shape (compare Figs. 4B and 5A). The profile of the equivalent cable, in turn, directly determines its impedance mismatch profile (Fig. 5B), which approximates the mean impedance mismatch at the same electrotonic location in the original morphology (the impedance mismatch profile would be preserved exactly for branches of semi-infinite length: compare *Eq. 2* and *Eq. 1*) (Clements and Redman 1989; Fleshman et al. 1988). Interestingly, the cumulative impedance mismatch in the equivalent cable provided the best predictor of backpropagation and forward propagation efficacy in 42 dendritic morphologies. This demonstrates that the equivalent cable transformation is a useful tool for predicting propagation of suprathreshold signals in active dendritic trees; this is remarkable given that it involves numerous approximations (Clements and Redman 1989; Fleshman et al. 1988). This result also suggests that the fate of a dendritic AP is usually not decided at a single branchpoint but rather depends on the accumulation of unfavorable impedance mismatches over many branchpoints (Manor et al. 1991).

Our finding that dendritic morphology has a significant impact on the propagation of APs in dendrites is in agreement with recent experimental evidence. Kim and Connors (1993) have shown that the efficacy of AP backpropagation in layer 5 pyramidal neurons is correlated with the number of apical oblique branches and the diameter of the apical trunk. In CA1 pyramidal neurons, a combination of calcium imaging and electrophysiological recordings has demonstrated that frequency-dependent attenuation of backpropagating APs is par-

ticularly severe in distal dendritic regions with extensive branching (Callaway and Ross 1995; Spruston et al. 1995). Finally, backpropagation in thalamocortical relay neurons appears to be less effective in dendrites that exhibit branching (Williams and Stuart 2000), again consistent with a key role for dendritic branching in determining propagation.

Modulation of AP propagation in dendrites

The densities of functional voltage-gated channels are subject to modulation by neurotransmitters, which can in turn affect backpropagation (Johnston et al. 1999). Our findings demonstrate that dendritic geometry places limits on the ability of backpropagation to be modulated in different neurons. As shown in Fig. 2, altering the density of dendritic Na^+ and K^+ channels over the same range can have strikingly diverse consequences on backpropagation in different morphologies. We predict that propagation of APs in different neurons, and in subregions of individual dendritic trees, will have different sensitivities to modulation of voltage-gated channels as a consequence of variations in morphology. In particular, neurons with an intermediate degree of dendritic branching, and dendritic regions exhibiting rapid increases in branching such as the apical tuft, should display the greatest sensitivity to modulation. This is testable experimentally as the functional density of different channel types can be varied pharmacologically to determine which morphologies are most sensitive to modulation. The consequences of use-dependent activation and inactivation of voltage-gated channels should also depend on dendritic morphology. Consistent with this idea, frequency-dependent attenuation of APs in dendrites (Callaway and Ross 1995; Spruston et al. 1995), which depends in part on a reduction in the effective Na^+ channel density (Colbert et al. 1997; Jung et al. 1997), is more pronounced in CA1 pyramidal neurons than in cortical pyramidal neurons (Stuart et al. 1997a), which exhibit less branching.

Dendritic geometry is not static but can change dramatically both during development and in adulthood (Bailey and Kandel 1993; McAllister 2000; Purves and Hadley 1985). In particular, a substantial increase in dendritic branching has been shown to be associated with neuronal maturation (Altman 1972; Berry and Bradley 1976; Kasper et al. 1994; Wu et al. 1999) and with activation of messenger pathways known to be involved in synaptic plasticity (Nedivi et al. 1998; Wu and Cline 1998; Yacoubian and Lo 2000). Our findings suggest that this increase in dendritic complexity will reduce backpropagation unless compensated by increases in voltage-gated channel densities. Consistent with this idea, there is substantial experimental evidence demonstrating that channel densities increase during development (Huguenard et al. 1988; MacDermott and Westbrook 1986; O'Dowd et al. 1988) in parallel with the changes in morphological complexity.

Finally our results point to an important role for dendritic spines in regulating AP propagation in dendrites (Baer and Rinzel 1991; Jaslove 1992). As spines can contribute more than 50% of the dendritic membrane area, the relationship between membrane area and propagation efficacy (Fig. 4) suggests that the changes in spine density that can occur during development (Gould et al. 1990; Harris et al. 1992) and synaptic plasticity (Engert and Bonhoeffer 1999; Maletic-Savatic et al. 1999) will also modulate the extent of propagation. This effect should be particularly pro-

nounced in neurons that also exhibit a high degree of dendritic branching. It is therefore interesting to note that neurons with minimal branching, such as dopamine neurons and interneurons, tend to be aspiny, while Purkinje cells, which exhibit a high degree of branching, have a very high spine density.

Implications for dendritic computation

Recent work has demonstrated that the backpropagating AP acts as a retrograde signal to dendritic synapses indicating that the axon has fired. This provides a coincidence detection mechanism that links postsynaptic APs and presynaptic activity to trigger synaptic plasticity (Häusser et al. 2000; Linden 1999; Stuart et al. 1997b). Our results show that since dendritic morphology limits the extent of propagation of dendritic APs, it defines the spatial range over which associations between synaptic inputs and APs can take place. In particular, we demonstrate that highly branching dendritic geometries do not permit strong coupling between axonal output and distal synapses, and thus in these neurons, the backpropagating AP cannot act as a global associative signal (Häusser et al. 2000; Larkum et al. 1999b; Linden 1999; Stuart et al. 1997b). Since such geometries are also poor substrates for forward propagation of APs (Figs. 6–8), synaptic integration in these neurons is far more dependent on local associations between inputs. Indeed such dendritic trees may be adapted to keep associations between inputs more localized to increase the number of independent sites of integration (Mel 1993). On the other hand, dendritic morphologies that favor propagation and are sensitive to modulation of propagation allow the associativity between output and input to be tuned over a wide range.

Our findings suggest that morphology will also influence the interaction between backpropagating APs and dendritically initiated APs. The initiation of dendritic APs requires strong and temporally synchronous synaptic input (Golding and Spruston 1998; Schiller et al. 1997; Stuart et al. 1997a), properties consistent with their role as coincidence detectors. However, in cortical pyramidal neurons, pairing backpropagating APs with distal synaptic input can substantially lower the threshold for initiation of dendritic APs; this can in turn lead to burst firing in the axon (Helmchen et al. 1999; Larkum et al. 1999a,b). By limiting the spatial spread of backpropagating and forward propagating APs, dendritic geometry should therefore play an important role in determining the sensitivity of individual neurons to coincident synaptic input as well as in defining the relationship between dendritic APs and neuronal output via the axon. Taken together, these considerations indicate that the tremendous diversity in dendritic morphology may have direct consequences for the computational strategies used by different neurons.

REFERENCES

ALTMAN J. Postnatal development of the cerebellar cortex in the rat. II. Phases in the maturation of Purkinje cells and of the molecular layer. *J Comp Neurol* 145: 399–463, 1972.

AMITAI Y, FRIEDMAN A, CONNORS BW, AND GUTNICK MJ. Regenerative activity in apical dendrites of pyramidal cells in neocortex. *Cereb Cortex* 3: 26–38, 1993.

BAER SM AND RINZEL J. Propagation of dendritic spikes mediated by excitable spines: a continuum theory. *J Neurophysiol* 65: 874–890, 1991.

BAILEY CH AND KANDEL ER. Structural changes accompanying memory storage. *Annu Rev Physiol* 55: 397–426, 1993.

BERRY M AND BRADLEY P. The growth of the dendritic trees of Purkinje cells in the cerebellum of the rat. *Brain Res* 112: 1–35, 1976.

BISCHOFBERGER J AND JONAS P. Action potential propagation into the presynaptic dendrites of rat mitral cells. *J Physiol (Lond)* 504: 359–365, 1997.

BUZSAKI G AND KANDEL A. Somadendritic backpropagation of action potentials in cortical pyramidal cells of the awake rat. *J Neurophysiol* 79: 1587–1591, 1998.

CALLAWAY JC AND ROSS WN. Frequency-dependent propagation of sodium action potentials in dendrites of hippocampal CA1 pyramidal neurons. *J Neurophysiol* 74: 1395–1403, 1995.

CHEN WR, MIDTGAARD J, AND SHEPHERD GM. Forward and backward propagation of dendritic impulses and their synaptic control in mitral cells. *Science* 278: 463–467, 1997.

CLEMENTS JD AND REDMAN SJ. Cable properties of cat spinal motoneurones measured by combining voltage clamp, current clamp and intracellular staining. *J Physiol (Lond)* 409: 63–87, 1989.

COLBERT CM, MAGEE JC, HOFFMAN DA, AND JOHNSTON D. Slow recovery from inactivation of Na⁺ channels underlies the activity-dependent attenuation of dendritic action potentials in hippocampal CA1 pyramidal neurons. *J Neurosci* 17: 6512–6521, 1997.

ENGERT F AND BONHOEFFER T. Dendritic spine changes associated with hippocampal long-term synaptic plasticity. *Nature* 399: 66–70, 1999.

FLESHMAN JW, SEGEV I, AND BURKE RB. Electrotonic architecture of type-identified alpha-motoneurons in the cat spinal cord. *J Neurophysiol* 60: 60–85, 1988.

GOLDING NL AND SPRUSTON N. Dendritic sodium spikes are variable triggers of axonal action potentials in hippocampal CA1 pyramidal neurons. *Neuron* 21: 1189–1200, 1998.

GOLDSTEIN SS AND RALL W. Changes of action potential shape and velocity for changing core conductor geometry. *Biophys J* 14: 731–757, 1974.

GOULD E, WOOLLEY CS, FRANKFURT M, AND MCEWEN BS. Gonadal steroids regulate dendritic spine density in hippocampal pyramidal cells in adulthood. *J Neurosci* 10: 1286–1291, 1990.

HARRIS KM, JENSEN FE, AND TSAO B. Three-dimensional structure of dendritic spines and synapses in rat hippocampus (CA1) at postnatal day 15 and adult ages: implications for the maturation of synaptic physiology and long-term potentiation. *J Neurosci* 12: 2685–2705, 1992.

HÄUSSER M, SPRUSTON N, AND STUART GJ. Diversity and dynamics of dendritic signaling. *Science* 290: 739–744, 2000.

HÄUSSER M, STUART G, RACCA C, AND SAKMANN B. Axonal initiation and active dendritic propagation of action potentials in substantia nigra neurons. *Neuron* 15: 637–647, 1995.

HELMCHEN F, SVOBODA K, DENK W, AND TANK DW. In vivo dendritic calcium dynamics in deep-layer cortical pyramidal neurons. *Nat Neurosci* 2: 989–996, 1999.

HINES ML AND CARNEVALE NT. The NEURON simulation environment. *Neural Comput* 9: 1179–1209, 1997.

HOFFMAN DA, MAGEE JC, COLBERT CM, AND JOHNSTON D. K⁺ channel regulation of signal propagation in dendrites of hippocampal pyramidal neurons. *Nature* 387: 869–875, 1997.

HOLMES WR. The role of dendritic diameters in maximizing the effectiveness of synaptic inputs. *Brain Res* 478: 127–137, 1989.

HUGUENARD JR, HAMILL OP, AND PRINCE DA. Developmental changes in Na⁺ conductances in rat neocortical neurons: appearance of a slowly inactivating component. *J Neurophysiol* 59: 778–795, 1988.

JACK JJB, NOBLE D, AND TSIEN RW. *Electric Current Flow in Excitable Cells.* Oxford, UK: Oxford Univ. Press, 1983.

JASLOVE SW. The integrative properties of spiny distal dendrites. *Neuroscience* 47: 495–519, 1992.

JOHNSTON D, HOFFMAN DA, COLBERT CM, AND MAGEE JC. Regulation of back-propagating action potentials in hippocampal neurons. *Curr Opin Neurobiol* 9: 288–292, 1999.

JOHNSTON D, MAGEE JC, COLBERT CM, AND CHRISTIE BR. Active properties of neuronal dendrites. *Annu Rev Neurosci* 19: 165–186, 1996.

JOYNER RW, MOORE JW, AND RAMON F. Axon voltage-clamp simulations. III. Postsynaptic region. *Biophys J* 15: 37–54, 1975.

JOYNER RW, WESTERFIELD M, AND MOORE JW. Effects of cellular geometry on current flow during a propagated action potential. *Biophys J* 31: 183–194, 1980.

JUNG HY, MICKUS T, AND SPRUSTON N. Prolonged sodium channel inactivation contributes to dendritic action potential attenuation in hippocampal pyramidal neurons. *J Neurosci* 17: 6639–6646, 1997.

KAMONDI A, ACSADY L, AND BUZSAKI G. Dendritic spikes are enhanced by cooperative network activity in the intact hippocampus. *J Neurosci* 18: 3919–3928, 1998.

KASPER EM, LÜBKE J, LARKMAN AU, AND BLAKEMORE C. Pyramidal neurons in layer 5 of the rat visual cortex. III. Differential maturation of axon targeting, dendritic morphology, and electrophysiological properties. *J Comp Neurol* 339: 495–518, 1994.

KIM HG AND CONNORS BW. Apical dendrites of the neocortex: correlation between sodium- and calcium-dependent spiking and pyramidal cell morphology. *J Neurosci* 13: 5301–5311, 1993.

LARKUM ME, KAISER KMM, AND SAKMANN B. Calcium electrogenesis in distal apical dendrites of layer 5 pyramidal cells at a critical frequency of back-propagating action potentials. *Proc Natl Acad Sci USA* 96: 14600–14604, 1999a.

LARKUM ME, ZHU JJ, AND SAKMANN B. A new cellular mechanism for coupling inputs arriving at different cortical layers. *Nature* 398: 338–341, 1999b.

LINDEN DJ. The return of the spike: postsynaptic action potentials and the induction of LTP and LTD. *Neuron* 22: 661–666, 1999.

LLINÁS RR. The intrinsic electrophysiological properties of mammalian neurons: insights into central nervous system function. *Science* 242: 1654–1664, 1988.

LLINÁS R AND SUGIMORI M. Electrophysiological properties of in vitro Purkinje cell dendrites in mammalian cerebellar slices. *J Physiol (Lond)* 305: 197–213, 1980.

LÜSCHER HR AND SHINER JS. Computation of action potential propagation and presynaptic bouton activation in terminal arborizations of different geometries. *Biophys J* 58: 1377–1388, 1990.

MACDERMOTT AB AND WESTBROOK GL. Early development of voltage-dependent sodium currents in cultured mouse spinal cord neurons. *Dev Biol* 113: 317–326, 1986.

MAGEE J, HOFFMAN D, COLBERT C, AND JOHNSTON D. Electrical and calcium signaling in dendrites of hippocampal pyramidal neurons. *Annu Rev Physiol* 60: 327–346, 1998.

MAINEN ZF, JOERGES J, HUGUENARD JR, AND SEJNOWSKI TJ. A model of spike initiation in neocortical pyramidal neurons. *Neuron* 15: 1427–1439, 1995.

MAINEN ZF AND SEJNOWSKI TJ. Influence of dendritic structure on firing pattern in model neocortical neurons. *Nature* 382: 363–366, 1996.

MALETIC-SAVATIC M, MALINOW R, AND SVOBODA K. Rapid dendritic morphogenesis in CA1 hippocampal dendrites induced by synaptic activity. *Science* 283: 1923–1927, 1999.

MANOR Y, KOCH C, AND SEGEV I. Effect of geometrical irregularities on propagation delay in axonal trees. *Biophys J* 60: 1424–1437, 1991.

MARTINA M, VIDA I, AND JONAS P. Distal initiation and active propagation of action potentials in interneuron dendrites. *Science* 287: 295–300, 2000.

MCALLISTER AK. Cellular and molecular mechanisms of dendrite growth. *Cereb Cortex* 10: 963–973, 2000.

MEL BW. Synaptic integration in an excitable dendritic tree. *J Neurophysiol* 70: 1086–1101, 1993.

MIGLIORE M, HOFFMAN DA, MAGEE JC, AND JOHNSTON D. Role of an A-type K⁺ conductance in the back-propagation of action potentials in the dendrites of hippocampal pyramidal neurons. *J Comput Neurosci* 7: 5–15, 1999.

NEDIVI E, WU GY, AND CLINE HT. Promotion of dendritic growth by CPG15, an activity-induced signaling molecule. *Science* 281: 1863–1866, 1998.

O'DOWD DK, RIBERA AB, AND SPITZER NC. Development of voltage-dependent calcium, sodium, and potassium currents in *Xenopus* spinal neurons. *J Neurosci* 8: 792–805, 1988.

OHME M AND SCHIERWAGEN A. An equivalent cable model for neuronal trees with active membrane. *Biol Cybern* 78: 227–243, 1998.

PARÉ D, LANG EJ, AND DESTEXHE A. Inhibitory control of somatodendritic interactions underlying action potentials in neocortical pyramidal neurons in vivo: an intracellular and computational study. *Neuroscience* 84: 377–402, 1998.

PARNAS I AND SEGEV I. A mathematical model for conduction of action potentials along bifurcating axons. *J Physiol (Lond)* 295: 323–343, 1979.

PASTUSHENKO VF, MARKIN VS, AND CHIZMADZHEV YA. Impulse propagation in a model of a non-uniform nerve fiber. III. Interaction of impulses in the area of a branching node of a nerve fiber. *Biofizika* 14: 883–890, 1969.

PAUWELUSSEN J. One way traffic of pulses in a neuron. *J Math Biol* 151: 151–172, 1982.

PRESS WH, TEUKOLSKY SA, VETTERLING WT, AND FLANNERY BP. *Numerical Recipes in C: The Art of Scientific Computing* (2nd ed.). Cambridge, UK: Cambridge Univ. Press, 1992.

PURVES D AND HADLEY RD. Changes in the dendritic branching of adult mammalian neurones revealed by repeated imaging in situ. *Nature* 315: 404–406, 1985.

RALL W. Theoretical significance of dendritic trees for neuronal input-output relations. In: *Neural Theory and Modeling,* edited by Reiss RF. Palo Alto, CA: Stanford Univ. Press, 1964, p. 73–97.

RAMON F, JOYNER RW, AND MOORE JW. Propagation of action potentials in inhomogeneous axon regions. *Fed Proc* 34: 1357–1363, 1975.

RAMÓN Y CAJAL S. *La Textura del Sistema Nerviosa del Hombre y los Vertebrados.* Madrid, Spain: Moya, 1904.

RAPP M, YAROM Y, AND SEGEV I. Modeling back propagating action potential in weakly excitable dendrites of neocortical pyramidal cells. *Proc Natl Acad Sci USA* 93: 11985–11990, 1996.

SCHILLER J, SCHILLER Y, STUART G, AND SAKMANN B. Calcium action potentials restricted to distal apical dendrites of rat neocortical pyramidal neurons. *J Physiol (Lond)* 505: 605–616, 1997.

SCHOPPA NE AND WESTBROOK GL. Regulation of synaptic timing in the olfactory bulb by an A-type potassium current. *Nat Neurosci* 2: 1106–1113, 1999.

SCHWINDT PC AND CRILL WE. Synaptically evoked dendritic action potentials in rat neocortical pyramidal neurons. *J Neurophysiol* 79: 2432–2446, 1998.

SEAMANS JK, GORELOVA NA, AND YANG CR. Contributions of voltage-gated Ca²⁺ channels in the proximal versus distal dendrites to synaptic integration in prefrontal cortical neurons. *J Neurosci* 17: 5936–5948, 1997.

SEGEV I. Single neurone models: oversimple, complex and reduced. *Trends Neurosci* 15: 414–421, 1992.

SEGEV I AND RALL W. Excitable dendrites and spines: earlier theoretical insights elucidate recent direct observations. *Trends Neurosci* 21: 453–460, 1998.

SHELTON DP. Membrane resistivity estimated for the Purkinje neuron by means of a passive computer model. *Neuroscience* 14: 111–131, 1985.

SPRUSTON N, SCHILLER Y, STUART G, AND SAKMANN B. Activity-dependent action potential invasion and calcium influx into hippocampal CA1 dendrites. *Science* 268: 297–300, 1995.

STUART G AND HÄUSSER M. Initiation and spread of sodium action potentials in cerebellar Purkinje cells. *Neuron* 13: 703–712, 1994.

STUART GJ AND SAKMANN B. Active propagation of somatic action potentials into neocortical pyramidal cell dendrites. *Nature* 367: 69–72, 1994.

STUART G, SCHILLER J, AND SAKMANN B. Action potential initiation and propagation in rat neocortical pyramidal neurons. *J Physiol (Lond)* 505: 617–632, 1997a.

STUART G AND SPRUSTON N. Determinants of voltage attenuation in neocortical pyramidal neuron dendrites. *J Neurosci* 18: 3501–3510, 1998.

STUART G, SPRUSTON N, SAKMANN B, AND HÄUSSER M. Action potential initiation and backpropagation in neurons of the mammalian CNS. *Trends Neurosci* 20: 125–131, 1997b.

SVOBODA K, DENK W, KLEINFELD D, AND TANK DW. In vivo dendritic calcium dynamics in neocortical pyramidal neurons. *Nature* 385: 161–165, 1997.

SVOBODA K, HELMCHEN F, DENK W, AND TANK DW. Spread of dendritic excitation in layer 2/3 pyramidal neurons in rat barrel cortex in vivo. *Nat Neurosci* 2: 65–73, 1999.

TURNER RW, MEYERS DE, RICHARDSON TL, AND BARKER JL. The site for initiation of action potential discharge over the somatodendritic axis of rat hippocampal CA1 pyramidal neurons. *J Neurosci* 11: 2270–2280, 1991.

WILLIAMS SR AND STUART GJ. Action potential backpropagation and somato-dendritic distribution of ion channels in thalamocortical neurons. *J Neurosci* 20: 1307–1317, 2000.

WU GY AND CLINE HT. Stabilization of dendritic arbor structure in vivo by CaMKII. *Science* 279: 222–226, 1998.

WU GY, ZOU DJ, RAJAN I, AND CLINE H. Dendritic dynamics in vivo change during neuronal maturation. *J Neurosci* 19: 4472–4483, 1999.

YACOUBIAN TA AND LO DC. Truncated and full-length TrkB receptors regulate distinct modes of dendritic growth. *Nat Neurosci* 3: 342–349, 2000.

YUSTE R, GUTNICK MJ, SAAR D, DELANEY KR, AND TANK DW. Ca²⁺ accumulations in dendrites of neocortical pyramidal neurons: an apical band and evidence for two functional compartments. *Neuron* 13: 23–43, 1994.

ZADOR AM, AGMON-SNIR H, AND SEGEV I. The morphoelectrotonic transform: a graphical approach to dendritic function. *J Neurosci* 15: 1669–1682, 1995.